DOI: https://doi.org/10.24425/amm.2025.156245

E.CH. CHEE YU⁰¹, S.S. CHE ABDULLAH^{01,2*}, I.H. WAN NORDIN⁰³, S.H. M.SALLEH^{®1}, R.A. MALEK^{®1,2}, P. PIETRUSIEWICZ^{®4}

ENHANCING SAMARIUM-DOPED CERIA ELECTROLYTES WITH MANGANESE FOR SOLID OXIDE FUEL CELL

This study focuses on synthesizing new electrolyte materials for solid oxide fuel cell (SOFC) with the composition of Ce_{0.8-x} $Mn_xSm_{0.2}O_{1.9-\delta}$ (x = 0, 0.025, 0.05, 0.1). The main aim is to investigate the effect of varying molar concentrations of manganese (Mn) as a secondary dopant on density, phase composition, and ionic conductivity of samarium-doped ceria (SDC). Accordingly, X-ray diffraction (XRD) and impedance spectroscopy (IS) were employed to characterize the samples. Mn-doped samples sintered at 1400°C for 5 hours exhibited a single-phase cubic fluorite structure with larger lattice parameters and volumes compared to the undoped sample. All samples achieved a high relative density exceeding 94%. Notably, the sample with 10 mol% Mn reached a relative density of 99.6%. Impedance data revealed that the ionic conductivity of the Mn-doped samples was enhanced by an order of magnitude compared to the undoped samples. This indicates that Mn is a promising dopant for SDC in electrolyte applications for SOFCs.

Keywords: Samarium oxide; transition element; solid electrolyte; conductivity; solid oxide fuel cell

1. Introduction

Solid oxide fuel cells (SOFCs) are a promising energy conversion technology due to their high efficiency, fuel flexibility, and environmental benefits [1-3]. A key factor in the performance of SOFCs is the development of effective solid electrolytes that exhibit high ionic conductivity at intermediate to low temperatures [4-6]. Among the potential candidates, ceria-based electrolytes, especially samarium-doped ceria (SDC), have gained significant attention. This is largely due to their superior ionic conductivity compared to traditional yttria-stabilized zirconia (YSZ) electrolytes, especially at reduced operating temperatures [7-9]. Nonetheless, ongoing research is focused on further enhancing the performance of SDC through strategic doping and compositional modifications [10-12].

Doping rare-earth dopants such as Sm, Gd, La, and Y into ceria-based electrolytes is a well-established approach. In addition, incorporating transition metal dopants into ceria-based electrolytes also has been shown to influence various material characteristics. This includes densification, grain growth, and ionic conductivity. Furthermore, recent studies have particularly explored the incorporation of transition metal dopants for example FeO₃, CuO, and V₂O₅ into the ceria lattice to enhance its ionic conductivity [13-17]. Among these, manganese (Mn) has demonstrated potential promise as an effective dopant due to its ability to substitute for the parent ions in the lattice. This modifies the crystal structure and influences the defect chemistry of the material. Notably, the substitution of Mn into Ce⁴⁺ sites may introduce lattice strain and promote the formation of oxygen vacancies to maintain charge neutrality. These vacancies acts as pathways for oxygen ion migration, which are crucial for facilitating the conduction of oxygen ions. It is also crucial to consider the potential electronic conductivity at higher Mn concentration, which can arise from Mn reduction due to its multiple oxidation states, should also be considered. Additionally, Mn enhances the sintering behavior of ceria-based materials, potentially leading to improved densification and, consequently, higher conductivity [18,19]. However, the precise mechanisms by which Mn doping affects the properties of SDC require further investigation.

Coressponding author: salmie@unimap.edu.my



UNIVERSITI MALAYSIA PERLIS (UNIMAP), FACULTY OF CHEMICAL ENGINEERING & TECHNOLOGY 02600 ARAU, PERLIS, MALAYSIA
UNIVERSITI MALAYSIA PERLIS (UNIMAP), CENTRE OF EXCELLENCE FOR FRONTIER MATERIALS RESEARCH (CFMR), JALAN KANGAR – ALOR SETAR, 01000 KANGAR, PERLIS,

UNIVERSITI MALAYSIA PERLIS (UNIMAP), FACULTY OF MECHANICAL ENGINEERING & TECHNOLOGY, KAMPUS TETAP PAUH PUTRA, 02600 ARAU, PERLIS, MALAYSIA

AV., 42-200 CZĘSTOCHOWA, POLAND

This research focuses on a series of $Ce_{0.8-x}Mn_xSm_{0.2}O_{1.9-\delta}$ (x=0,0.025,0.05, and 0.1) samples with varying Mn concentrations. In this study, the Sm doping ratio was fixed at 20 mol% to specifically investigate the effect of Mn doping in Ce. A comprehensive characterization approach was employed to investigate the impact of Mn doping on the crystal structure, phase composition, densification, and electrical conductivity of SDC. By exploring the relationship between Mn concentration, crystal structure, and ionic conductivity, we aim to identify optimal doping strategies for enhancing the performance of SDC electrolytes.

2. Experimental

Samples with the formula of $Ce_{0.8-x}Mn_xSm_{0.2}O_{1.9-\delta}$ (x=0,0.025,0.05, and 0.1) were synthesized using cerium (II) oxide, CeO_2 (99.9% purity, Acros Organics), samarium (III) oxide, Sm_2O_3 (99.95% purity, Sigma Aldrich), and manganese (IV) oxide, MnO_2 (99% purity, Acros Organics) via conventional solid-state reaction. The raw materials were weighed accurately according to their stoichiometry. Consequently, they were mixed with ethanol for 1 hour to acquire a homogenous mixture. The mixed powder was then pressed uniaxially under 3000 psi for 5 minutes into pellets with a diameter of 15 mm and a thickness of 4 to5 mm. The pellets were subsequently sintered at 1400°C under an air atmosphere. TABLE 1 presents the chemical composition and abbreviation of prepared samples.

TABLE 1 Composition of $Ce_{0.8-x}Mn_xSm_{0.2}O_{1.9-\delta}$ (x = 0, 0.025, 0.05, 0.10)

Sample	Composition	Sample Abbreviation	Mn mol%
1	$Ce_{0.8}Sm_{0.2}O_{1.9-\delta}$	SDC	0
2	$Ce_{0.775}Mn_{0.025}Sm_{0.2}O_{1.9-\delta}$	SDC-Mn2.5	2.5
3	$Ce_{0.75}Mn_{0.05}Sm_{0.2}O_{1.9-\delta}$	SDC-Mn5.0	5.0
4	$Ce_{0.70}Mn_{0.1}Sm_{0.2}O_{1.9-\delta}$	SDC-Mn10.0	10.0

The phase composition and crystalline structure of the sintered samples were analyzed using powder X-ray diffraction (XRD). For this purpose, a Bruker D2 Phaser x-ray diffractometer was used, operating over a 2θ range of 20° to 80° with a scanning rate of 0.02° /sec, employing Cu– K_{α} radiation with a wavelength of 1.54 Å. In a separate crystal structure analysis, X'pert Highscores Plus was utilized to determine the crystalline phases, lattice parameters, and unit cell volume.

The density of the sintered samples was determined using the Archimedes method, which involved measuring the mass of the sample in water to calculate the apparent density. This apparent density was then compared to the theoretical density derived from lattice parameters obtained through XRD analysis. By comparing these two values, the relative density of the samples was calculated, providing insight into the degree of densification achieved during the sintering process.

Impedance measurements were conducted using LCR meter (HIOKI IM353) to determine the electrical conductiv-

ity of the sintered samples. Prior to measurement, the samples were polished using 800 to 1200-grit number abrasive paper to achieve a smooth surface. A layer of silver paste was applied to the polished surfaces, followed by heat treatment at 600°C for 1 hour to act as a current collector. Subsequently, two-point probe technique was applied during impedance measurements, which were conducted over a frequency range of 10 to 1 MHz. The temperature-dependent conductivity was evaluated from 300°C to 800°C, with data collected at 100°C intervals. Samples were held at measurement temperature for 1 hour to ensure thermal equilibrium. Simultaneosly, a custom-designed alumina sample holder equipped with high-purity platinum plates and wires was used as both current and voltage electrodes, ensuring minimal contact resistance within a high-temperature furnace.

3. Results and discussions

The XRD patterns of $Ce_{0.8-x}Mn_xSm_{0.2}O_{1.9-\delta}$ (where x=0, 0.025, 0.05, and 0.1) samples with varying Mn doping concentrations are presented in Figure 1. The patterns reveal distinct changes in the SDC-Mn samples compared to the Mn-undoped SDC sample. Notably, as shown in Fig. 1(b), (c), and (d), the undoped SDC sample exhibits additional peaks at 2 theta = 28.30°, 33.07°, 47.14° and 56.00°, indicating the presence of a secondary phase. These additional peaks are absent in the SDC-Mn samples. This suggest that within the studied concentration range (2.5 to 10.0 mol%), Mn is successfully incorporated into the CeO2 lattice, forming a solid solution. This observation confirms that all SDC-Mn samples exhibit a single-phase structure, with all diffraction peaks corresponding to the cubic fluorite crystal structure of doped ceria (ICDD 01-075-0158) with the space group Fm3m.

Further analysis indicates that the secondary phase in the Mn-undoped SDC sample corresponds to the Sm₂O₃ phase (ICDD 03-065-3183). Considering that all samples were sintered under identical conditions (1400°C, 5 hours, heating rate 10°C/min), the findings suggest that Mn doping promotes the reaction and sintering processes among the constituent elements [20-22]. These results indicate that Mn doping significantly modifies the crystal structure and phase stability, positioning Mn as a beneficial dopant for ceria-based material.

Moreover, as presented in the magnified patterns in Fig. 1(c), the XRD patterns of the SDC-Mn samples reveal a progressive shift of peaks to higher angles with increasing Mn content. This shift indicates an increase in lattice strain, leading to a corresponding decrease in lattice parameters. As the samples possess a cubic structure, the unit cell volume decreases proportionally. Notably, th reduction in lattice parameter with increasing Mn content is attributed to the substitution of smaller Mn⁴⁺ ions (ionic radius 0.53 Å) for the larger Ce⁴⁺ ions (0.93 Å) [23]. Fig. 2 and TABLE 2 compare the lattice parameter and unit cell volume of the SDC and SDC-Mn samples. The Mn-undoped SDC sample exhibits mixed phases has a smaller lattice parameter and unit cell volume compared to the SDC-Mn samples. Mn doping up

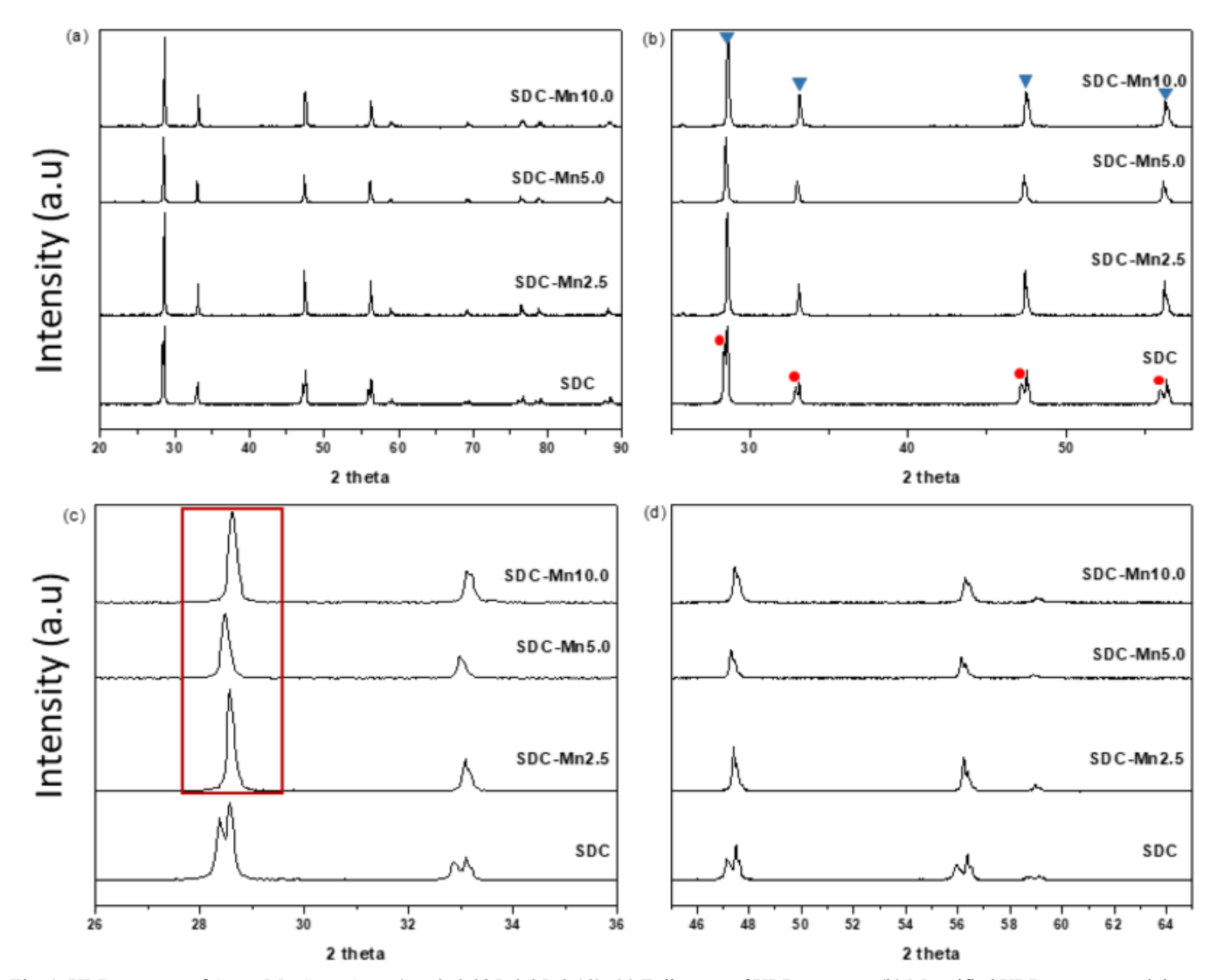


Fig. 1. XRD patterns of $Ce_{0.8-x}Mn_xSm_{0.2}O_{1.9-\delta}(x=0,0.025,0.05,0.10)$: (a) Full range of XRD patterns, (b) Magnified XRD patterns, red dot assigned for secondary peaks, (c) Magnified XRD patterns at lower range, red line shows peak shifting, (d) Magnified XRD pattern at higher range

to 2.5 mol% increases the lattice parameter and unit cell volume, while further doping results in a decrease in cell size.

The densities of the SDC and SDC-Mn samples are presented in TABLE 2. In particular, the density of the SDC-Mn

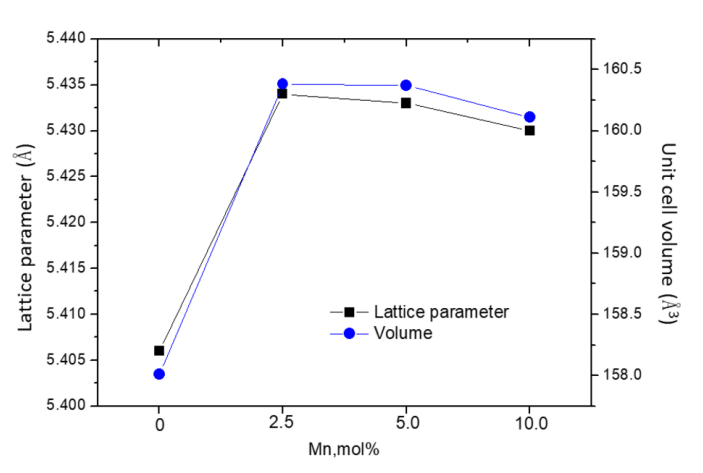


Fig. 2. Lattice parameter and unit cell volume of $Ce_{0.8-x}Mn_xSm_{0.2}O_{1.9-\delta}$ (x = 0, 0.025, 0.05, 0.10)

TABLE 2 XRD analysis data and relative density of $Ce_{0.8-x}Mn_xSm_{0.2}O_{1.9-\delta}$ (x = 0, 0.025, 0.05, 0.10)

Sample Abbreviation	Lattice parameter, Å	Unit cell volume, Å ³	Relative density, %
SDC	5.406	158.01	94.6
SDC-Mn2.5	5.434	160.38	96.7
SDC-Mn5.0	5.433	160.37	99.2
SDC-Mn10.0	5.430	160.38	99.6

samples increased to over 96% of the theoretical values, in contrast to the SDC samples, which exhibited a lower relative density of 94.6%. This suggests that the Mn dopant significantly enhanced the densification of the samples. The improvement can be attributed to the viscous flow mechanism, where the presence of the dopant reduced friction for mass transport at inter-particle and grain boundaries. Similar findings have been reported in previous studies on the effects of transition metal elements on density [13,23].

The Arrhenius plot in Fig. 3 illustrates the temperature dependence of conductivity for SDC and SDC-Mn samples. The graph reveals that SDC-Mn samples exhibit higher conductivity compared to SDC samples. Meanwhile, the lower conductivity observed in the SDC sample is attributed to the presence of a mixed phase, potentially an impurity phase, which may contribute to the reduced conductivity. Additionally, the lower density of the SDC sample, as shown in TABLE 2, is another factor, as the higher porosity of polycrystalline solid electrolytes adversely impacts ionic conductivity by reducing the effective conducting area [24,25]. Nevertheless, this factor is minimal due to the intrinsic properties of the material, with the specific type of dopants, particularly Mn, in this study playing a more significant role in determining conductivity.

In contrast, all SDC-Mn samples exhibit a remarkable enhancement in conductivity, exceeding two orders of magnitude,

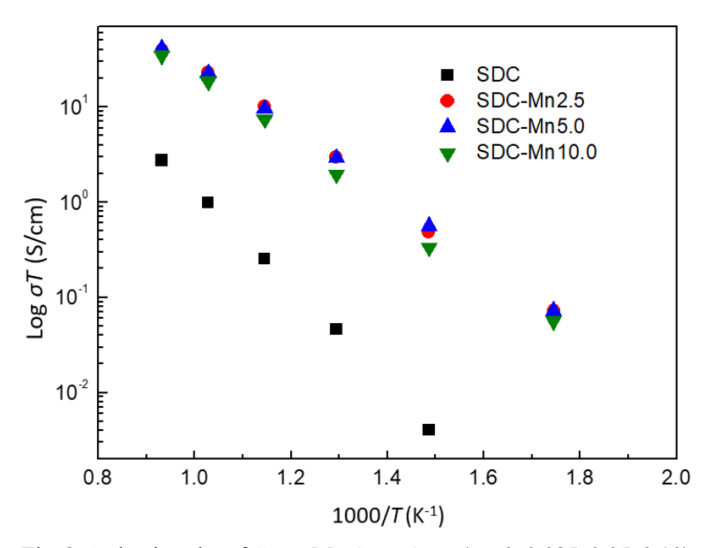


Fig. 3. Arrhenius plot of $Ce_{0.8\text{-x}}Mn_xSm_{0.2}O_{1.9\text{-}\delta} (x$ = 0, 0.025, 0.05, 0.10) measured at 300-800°C

particularly at lower temperatures below 500°C. The degree of this conductivity enhancement decreases as temperature increases, indicating that the effect of Mn doping is more pronounced at lower temperatures. Activation energies (E_a) were estimated from the Arrhenius equation as follows,

$$\sigma T = \sigma_0 \exp(-E_a/kT) \tag{1}$$

where σ_0 is a pre-exponential factor that reflects the effective number of mobile charge carriers, σ is ionic conductivity, T is absolute temperature, and k is Boltzmann constant, and E_a represents the activation energy. The relationship between Mn concentration, conductivity, and estimated activation energies, E_a , is presented in Fig. 4. This figure offers an overview of the relationship between compositions, conductivity, and activation energy in these samples. From Fig. 4(a), a significant increase in conductivity is observed from SDC to SDC-Mn2.5, while SDC-Mn2.5 and SDC-Mn5.0 exhibit comparable conductivity values. The peak conductivity is attained within the 2.5-5.0 mol% range of Mn concentration. However, when the Mn concentration is further increased to SDC-Mn10.0, there is a slight decline in conductivity. This phenomenon is commonly observed in polycrystalline materials and can be attributed to the interactions between dopants and the defect structure beyond the optimal doping level, which reduces the mobility of charge carriers and consequently lowers conductivity [26,27].

Comparing the conductivity values in Fig. 4(a) and activation energies in Fig. 4(b) reveals that doping SDC with Mn results in lower E_a than pure SDC. This observation aligns with the Arrhenius equation, as E_a is inversely proportional to conductivity. Notably, the lower E_a implies a reduced energy barrier for ion conduction, resulting in higher conductivity.

The correlation between Mn concentration, cell volume, and conductivity reveals a consistent trend: samples with larger cell volumes tend to exhibit higher conductivity, as can be seen

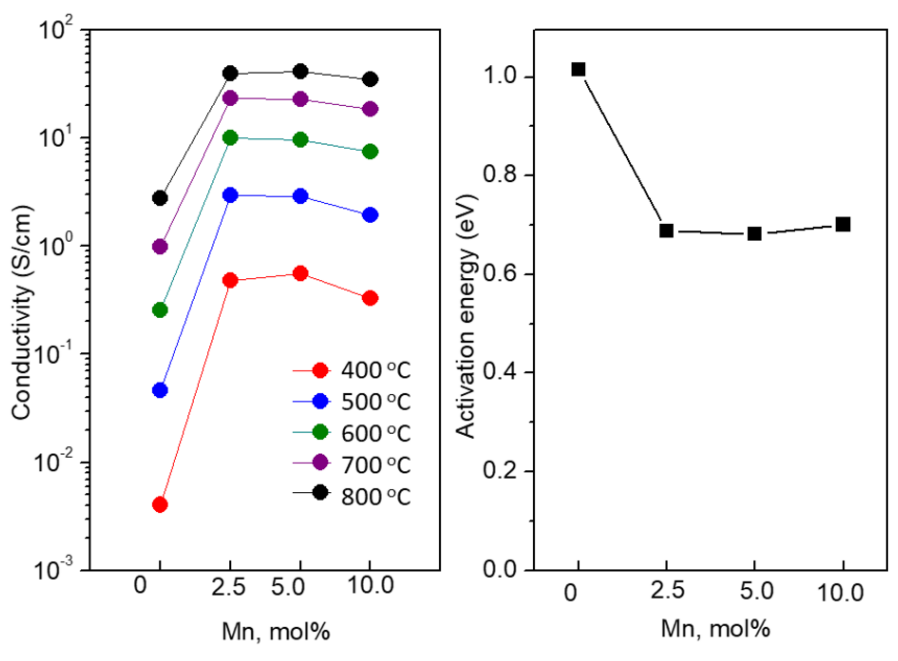


Fig. 4. (a) Conductivity versus Mn concentration, (b) Activation energy of Ce_{0.8-x}Mn_xSm_{0.2}O_{1.9-δ}

in Fig. 5. Previous research reported that lattice distortions, such as those induced by altering the composition or structure of the material, can lower the energy barriers for ion migration. This makes it easier for ions to move through the lattice, thereby enhancing ionic conductivity. This suggests that modifying the lattice structure influences the mobility of charge carriers, facilitating their movement through the lattice [28]. These findings underscore the importance of strategic dopant selection and incorporation in significantly enhancing a material's conductivity.

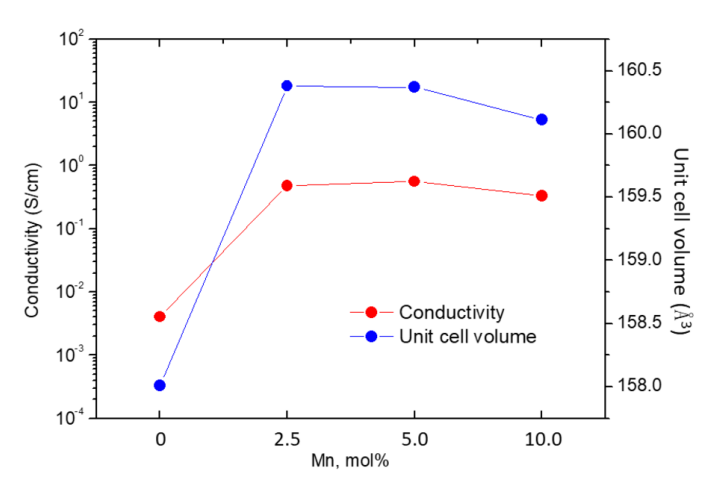


Fig. 5. Correlation between conductivity and unit cell volume of $Ce_{0.8-x}Mn_xSm_{0.2}O_{1.9-\delta}$

4. Conclusion

In this study, the effects of Mn doping on the structural, densification, and electrical properties of Ce_{0.8-x}Mn_xSm_{0.2}O_{1.9-δ} samples were investigated. XRD analysis revealed that Mn doping successfully eliminates secondary phases observed in SDC sample without Mn doping. This led to the incorporation of Mn into the CeO2 lattice and formation of a single-phase cubic fluorite structure across the studied doping range. Meanwhile, Mn doping also led to a marked increase in sample density. Furthermore, Mn doping resulted in enhanced conductivity, particularly at lower temperatures. Notably, Mn doping reduced the activation energy for oxygen ion migration, significantly contributing to improved conductivity. At the same time, the optimal Mn concentration for peak conductivity lies between 2.5 and 5.0 mol%. In essense, these findings demonstrate that Mn doping in ceria-based electrolyte effectively enhances structural homogeneity, densification, and electrical performance. This, ultimately, makes it a promising strategy for optimizing materials in SOFC applications and other electrochemical devices.

Acknowledgement

The authors would like to acknowledge the support from the Fundamental Research Grant Scheme (FRGS) under a grant number of FRGS/1/2020/STG05/UNIMAP/02/4 from the ministry of Higher Education (MoHE) Malaysia.

REFERENCES

- [1] A. Choudhury, H. Chandra, A. Arora, Recent advances in solid oxide fuel cells (SOFCs): A review. Renew. Sustain. Energy Rev. **20**, 430-442 (2013).
 - DOI: https://doi.org/10.1016/j.rser.2012.11.031
- [2] S.C. Singhal, Advances in solid oxide fuel cell technology. Solid State Ion. 135, 305-313 (2000).
 - DOI: https://doi.org/10.1016/s0167-2738(00)00452-5
- [3] A.B. Stambouli, E. Traversa, Solid oxide fuel cells (SOFCs): A review of the state-of-the art. Renew. Sustain. Energy Rev. 6 (5), 433-455 (2002).
 - DOI: https://doi.org/10.1016/s1364 0321(02)00014-x
- [4] A. Ndubuisi, S. Abouali, K. Singh, V. Thangadurai, Progress and perspectives in solid-state electrolytes for next-generation solid oxide fuel cells. J. Mater. Chem. A. 10 (5), 2196-2227 (2022). DOI: https://doi.org/10.1039/d1ta08475e
- J. Patakangas, Y. Ma, Y. Jing, P.D. Lund, Recent advances in anode materials for intermediate temperature solid oxide fuel cells.
 J. Power Sources. 263, 315-331 (2014).
 - DOI: https://doi.org/10.1016/j.jpowsour.2014.04.008
- [6] O. Chun, F. Jamshaid, M.Z. Khan, O. Gohar, I. Hussain, Y. Zhang, K. Zheng, M. Saleem, M. Motola, M.B. Hanif, Recent advances in electrolyte materials for solid oxide fuel cells. J. Power Sources. 610, 234719 (2024).
 - DOI: https://doi.org/10.1016/j.jpowsour.2024.234719
- B.C.H. Steele, A. Heinzel, Materials for fuel-cell technologies.
 Nat. 414 (6861), 345-352 (2001).
 DOI: https://doi.org/10.1038/35104620
- [8] B. Wang, B. Zhu, S. Yun, W. Zhang, C. Xia, M. Afzal, Y. Cai, Y. Liu, Y. Wang, H. Wang, Highly efficient and durable anode materials for solid oxide fuel cells. NPG Asia Mater. 11, 51 (2019). DOI: https://doi.org/10.1038/s41427-019-0152-8
- [9] K. Manakor, S.M. Jamil, M.H.D. Othman, M.A. Rahman, J. Jaafar, A.F. Ismail, Effects of NiO-YSZ cermet anode compositions on the performance of planar solid oxide fuel cell (SOFC). J. Teknol. 70 (2) (2014).
 - DOI: https://doi.org/10.11113/jt.v70.3432
- [10] S.S.C. Abdullah, J.X. Soong, M.Z.B.M. Yusoff, S.H. Salleh, R.A. Malek, Synthesis and characterization of strontium doped lanthanum gallate as electrolyte for intermediate temperature solid oxide fuel cells. Key Eng. Mater. 930, 9-14 (2022). DOI: https://doi.org/10.4028/p-v3fpd1
- [11] K. Venkataramana, C. Madhuri, C. Madhusudan, A. Bhogi, B. Srinivas, C.V. Reddy, Synthesis and characterization of Sm0.2 Ce0.8O1.9-δ electrolyte for intermediate temperature solid oxide fuel cells. Mater. Sci. Semicond. Process. 142, 106495 (2022). DOI: https://doi.org/10.1016/j.mssp.2022.106495
- [12] J. Zolhafizi, M.A. Azmi, H. Rahman, H. Zakaria, S. Hassan, S. Mahzan, A. Ismail, A.M.T. Ariffin, M.F. Tukimon, U.A. Yusof, N.A. Baharuddin, Review on the development of proton conducting solid oxide fuel cells (PC-SOFCs) for low-temperature applications. J. Kej. 35 (1), 65-76 (2023).
 - DOI: https://doi.org/10.17576/jkukm-2023-35(1)-07

- [13] C. Fu, Q. Liu, S.H. Chan, X. Ge, G. Pasciak, Development of anode-supported planar SOFC with thin film YSZ electrolyte. Int. J. Hydrogen Energy 35 (20), 11200-11207 (2010). DOI: https://doi.org/10.1016/j.ijhydene.2010.07.049
- [14] S. Hussain, Y. Li, K.H. Thebo, Z. Ali, M. Owais, S. Hussain, Anode materials for solid oxide fuel cells: A review. Mater. Chem. Phys. 267, 124576 (2021).
 - DOI: https://doi.org/10.1016/j.matchemphys.2021.124576
- [15] T. Nishimura, T. Kodama, S. Genta, T. Ishii, Effect of preparation method on the structural and electrical properties of gadoliniumdoped ceria electrolytes. Sci. Rep. 12 (1), 10103 (2022). DOI: https://doi.org/10.1038/s41598-022-14180-3
- [16] S.Y. Toor, E. Croiset, Review of proton conducting solid oxide fuel cells (PC-SOFCs) with emphasis on electrolyte materials. Ceram. Int. 46 (1), 1148-1157 (2020). DOI: https://doi.org/10.1016/j.ceramint.2019.09.083
- Y. Zheng, M. Zhou, L. Ge, S. Li, H. Chen, L. Guo, Effect of Ni content on the performance of Ni-YSZ cermet anodes for SOFCs.
 J. Alloys Compd. 509 (2), 546-550 (2011).
 DOI: https://doi.org/10.1016/j.jallcom.2010.09.103
- [18] R. Basumatary, S. Sahu, D. Goyari, D. Pamu, R.K. Brahma, Recent advances in mixed ionic and electronic conducting materials for solid oxide fuel cells. J. Alloys Compd. 999, 174958 (2024). DOI: https://doi.org/10.1016/j.jallcom.2024.174958
- [19] D. Amaral, M. Assis, L. Rocha, E. Longo, C. Aldao, P. Desimone, M. Teodoro, C. Macchi, H. Nascimento, A. Somoza, M. Ponce, F. Moura, Synthesis and characterization of strontium doped lanthanum cobalt ferrite for solid oxide fuel cell cathodes. Ceram. Int. 50 (9), 16532 16539 (2024). DOI: https://doi.org/10.1016/j.ceramint.2024.02.142
- [20] S. Park, H. Yoo, Electrical conductivity of ceria-based electrolytes for intermediate temperature solid oxide fuel cells. Solid State Ion. 176 (15-16), 1485-1490 (2005).

DOI: https://doi.org/10.1016/j.ssi.2005.03.015

- [21] H. Song, J.C. Yoon, R. Kim, J. Im, S. Lee, J. Ryu, Recent progress in metal-supported solid oxide fuel cells. Ceram. Int. **49** (16), 26719-26725 (2023).
 - DOI: https://doi.org/10.1016/j.ceramint.2023.05.207
- [22] P. Venkataswamy, D. Jampaiah, D. Mukherjee, C.U. Aniz, B.M. Reddy, Recent advances in nanostructured anode materials for solid oxide fuel cells: A review. Catal. Lett. 146 (10), 2105-2118 (2016).
 - DOI: https://doi.org/10.1007/s10562-016-1811-9
- [23] J. Hong, S. Ida, T. Ishihara, Perovskite-type oxides as cathode materials for solid oxide fuel cells. Solid State Ion. 32, 374-377 (2014).
 - DOI: https://doi.org/10.1016/j.ssi.2013.11.049
- [24] E.J. Cheng, M. Liu, Y. Li, T. Abe, K. Kanamura, Recent progress on high-performance electrolyte materials for solid oxide fuel cells. J. Power Sources. 517, 230705 (2022).
 - DOI: https://doi.org/10.1016/j.jpowsour.2021.23070558
- [25] Z. Luo, C. Qin, W. Xu, H. Liang, W. Lei, X. Shen, A. Lu, Anode materials for solid oxide fuel cells: A review. Ceram. Inter. 46 (10), 15613-15620 (2020).
 - DOI: https://doi.org/10.1016/j.ceramint.2020.03.108
- [26] J.W. Fergus, Electrolytes for solid oxide fuel cells. J. Power Sources 162 (1), 30-40 (2006).DOI: https://doi.org/10.1016/j.jpowsour.2006.06.062
- [27] Z. Li, T. Mori, J. Zou, J. Drennan, Ceria-based materials for solid oxide fuel cells. Phys. Chem. Chem. Phys. 14 (23), 8369 (2012). DOI: https://doi.org/10.1039/c2cp40845g
- [28] K. Kim, D.J. Siegel, First-principles study of mixed ionic–electronic conducting perovskites for solid oxide fuel cell cathodes. J. Mater. Chem. A 7 (7), 3216-3227 (2019). DOI: https://doi.org/10.1039/c8ta10989c